









SOCA-CFAR Processor in A Homogeneous Erlang-Distributed Clutter: Exact Closed-Form Expression for the P_{fa}

Abdelhalim Rabehi^{1*}, El-Hadi Meftah², Slimane Benmahmoud^{1,3}, Abdelaziz Rabehi¹, Amal H. Alharbi⁴,
El-Sayed M. El-Kenawy^{5,6}

¹Laboratory of Telecommunication and Smart Systems (LTSS), Faculty of Science and Technology, University of Djelfa, Djelfa 17000, Algeria

²LISIC Laboratory, Faculty of Electrical Engineering, University of Science and Technology Houari Boumediene, Algiers 16111, Algeria

³Department of Electronic Engineering, University of M'sila, M'sila 28000, Algeria

⁴Department of Computer Sciences, College of Computer and Information Sciences, Princess Nourah bint Abdulrahman University, Riyadh 11671, Saudi Arabia

⁵School of ICT, Faculty of Engineering, Design and Information & Communications Technology (EDICT), Bahrain Polytechnic, Manama 815, Bahrain

⁶Applied Science Research Center, Applied Science Private University, Amman 11937, Jordan

Corresponding Author Email: abdelaziz.rabehi@univ-djelfa.dz

Copyright: ©2025 The authors. This article is published by IETA and is licensed under the CC BY 4.0 license (<http://creativecommons.org/licenses/by/4.0/>).

<https://doi.org/10.18280/ts.420328>

ABSTRACT

Received: 5 April 2025

Revised: 10 May 2025

Accepted: 17 June 2025

Available online: 30 June 2025

Keywords:

CFAR processors, SOCA-CFAR, probability of false alarm (P_{FA}), erlang-distributed clutter, hypothesis testing

In this work, we have derived a closed-form expression for the probability of false alarm (P_{FA}) of the smallest-of cell-averaging constant false alarm rate (SOCA-CFAR) processor which operates in a homogeneous Erlang-distributed clutter environment. This expression indicates that the P_{FA} is independent of the rate parameter λ of the Erlang clutter. Moreover, as an intermediate step, we have derived accurate formulations for the probability density function (PDF) for the sum and the minimum sum of independent and identically distributed (i.i.d) Erlang random variates. The numerical simulations stipulate an enhancement in the SOCA-CFAR's P_{FA} as the shape parameter k of the Erlang clutter increases. The accuracy of the analytical outcomes presented in this work is corroborated through Monte Carlo simulations.

1. INTRODUCTION

In radar target detection, undesirable reflections from objects are termed clutter. In homogeneous clutter backgrounds, constant false alarm rate (CFAR) techniques are fundamental for maintaining a predetermined, consistent false alarm rate (FAR) [1-5].

A CFAR processor determines the optimal detection threshold by analyzing the clutter level. This analysis involves processing a set of strategically positioned reference cells surrounding the cell under investigation (CUI), also known as the test cell. By carefully examining these reference cells, the CFAR processor generates a robust estimate of the clutter magnitude, effectively differentiating between the signal of interest and unwanted clutter. This process is crucial for mitigating false alarms while preserving the sensitivity needed for effective target detection and tracking in radar systems.

The cell averaging (CA)-CFAR processor is a well-known CFAR variant [6, 7]. It methodically estimates the clutter's mean level by averaging the values from all cells surrounding the CUI. This comprehensive averaging approach provides a robust estimate of the average clutter magnitude, enabling effective signal-clutter discrimination. Numerous CFAR

variants have been developed for specific operational contexts. These include the greatest-of (GO) CA-CFAR processor, introduced by some researchers [8, 9] to manage false alarm rates in clutter transition zones; the smallest-of (SO) CA-CFAR processor, described by Trunk (1978) and elaborated in later studies [10-13]; the ordered statistics OS-CFAR processor, proposed by Rohling (1983) and refined in subsequent research [14, 15]; and the Variability Index CFAR (VI-CFAR) introduced by Guida et al. [16]. Each of these variants offers distinct advantages and trade-offs. The OS-CFAR processor offers robustness against interfering targets through rank-based threshold estimation; however, it incurs computational overhead due to sorting operations. VI-CFAR adapts to clutter heterogeneity by exploiting statistical variability measures, achieving superior performance in mixed clutter environments at the cost of increased computational complexity ($\sim 10^4$ operations per decision). Despite these advances, systematic comparative analysis of these processors under Erlang-distributed clutter—particularly relevant for maritime and urban radar scenarios—is lacking in existing literature. Most studies focus on Weibull or K-distributed clutter models, leaving a gap in understanding optimal CFAR selection for Erlang environments. This limitation motivates

the need for comprehensive performance evaluation that considers both detection capability and computational efficiency, enabling informed processor selection for specific operational scenarios. These diverse CFAR implementations collectively underscore the critical importance of selecting appropriate statistical models for optimal radar performance.

This modeling challenge has become increasingly complex with the evolution of contemporary high-resolution radar systems. The radar research community has developed several compelling non-Gaussian statistical models specifically for high-resolution radar clutter, including Positive Alpha-Stable, Weibull, Log-Normal, Pareto, and K-distributions [16-22]. These models offer more accurate representations of clutter behavior. Researchers are actively investigating the most appropriate model for capturing the complexities of clutter dynamics in high-resolution radar environments. Utilizing these sophisticated models can significantly enhance clutter mitigation strategies, improving target detection accuracy and overall system performance in complex operational scenarios.

However, incorporating certain non-Gaussian models into CFAR frameworks creates difficulties in deriving the clutter mean level estimate. This limitation significantly impacts the assessment of CFAR detector performance using key metrics such as probability of detection and false alarm probability. With non-Gaussian clutter models, deriving closed-form expressions for these performance metrics is often impossible, making numerical evaluation necessary, which may not always be feasible. This complexity underscores the inherent trade-off between sophisticated clutter modeling and the practical challenges of evaluating and deploying CFAR schemes in real-world radar systems. Continued research into novel methodologies is crucial for improving the performance and reliability of CFAR techniques across diverse radar applications.

In some studies [23, 24], a meticulous examination of the CA- and GOCA-CFAR processors' performance was conducted, presuming a scenario characterized by homogeneous Gamma-distributed clutter. These investigations yielded valuable insights, with the authors deriving expressions for the probability of false alarm (P_{FA}) in the form of definite integrals specific to these CFAR processors. Building upon this groundwork, the authors in [25] have made a step forward by providing closed-form formulations for the integral-form PFA expressions given in [23, 24].

Inspired by the contributions in the aforementioned papers, in this work, we will derive a closed-form expression for the P_{FA} of the SOCA-CFAR processor in the presence of a homogeneous Erlang-distributed clutter.

The rest of this paper is organized as follows: In the next section, we will give a brief overview of the SOCA-CFAR processor and we recall the Erlang distribution. Some important findings and novel statistics for the clutter's mean level will be presented in Section 3. These findings will be later utilized in Section 4 to conduct an analytical assessment of the SOCA-CFAR processor's P_{FA} . Section 5, will provide and detailly discuss some important numerical results. At last, a conclusion will be presented in Section 4.

2. SOCA-CFAR PROCESSING AND THE ERLANG DISTRIBUTION

In this section, we give a brief overview of the SOCA-

CFAR processor and we callback the Erlang distribution.

2.1 SOCA-CFAR processor's description and related assumptions

In a SOCA-CFAR processor, the statistic Z of its output, which represents an estimate of the clutter's level, is given by

$$Z = \frac{1}{N} \min(Z_1, Z_2) \quad (1)$$

where, $Z_1 = \sum_{i=1}^N X_i$ and $Z_2 = \sum_{i=N+1}^{2N} X_i$ are the sums of the leading and lagging windows, respectively. $X_i, i \in \{1, 2, \dots, 2N\}$ represent the contents of the reference cells surrounding the cell under investigation (CUI) whose content is X_0 . N denotes the size of the reference window.

A binary test to declare the presence or absence of a target can be given by

$$\begin{aligned} H_1 &: X_0 > TZ \\ H_0 &: X_0 < TZ \end{aligned} \quad (2)$$

where, H_0 and H_1 represent the target-absent and target-present hypothesis, respectively. T is the scaling factor.

2.2 Erlang distribution

Erlang distribution is a two-parameter distribution and is used in statistical modeling in many fields of engineering and sciences.

Definition 1 (Erlang RV). A RV X that is Erlang-distributed with a shape k and a rate λ is denoted by $X \sim \text{Erlang}(k, \lambda)$. Its PDF and CDF using the shape-rate parametrization are given, respectively, by

$$f_X(x) = \frac{\lambda^k x^{k-1} e^{-\lambda x}}{(k-1)!} \text{ for } x \geq 0 \quad (3)$$

$$F_X(x) = \frac{\gamma(k, \lambda x)}{(k-1)!} \text{ for } x \geq 0 \quad (4)$$

with $k \in \{1, 2, 3, \dots\}$ and $\lambda \in (0, \infty)$.

3. NOVEL IMPORTANT STATISTICS

In this section, we introduce some important statistics, that we will be utilized later in the next section, when evaluate the SOCA-CFAR processor's P_{FA} .

Lemma 1 (Sum of *i.i.d* Erlang variates).

Let $\{X_i\}_{i=1}^{2N}$ be a sequence of *i.i.d* RVs for which $X_i \sim \text{Erlang}(k, \lambda)$. The PDF and CDF of the RV

$$Z = \sum_{i=1}^{2N} X_i \quad (5)$$

are given, respectively, by:

$$f_Z(z) = \frac{\lambda^{2Nk}}{(2Nk-1)!} z^{2Nk-1} e^{-\lambda z}, \quad z > 0, \quad (6)$$

$$F_Z(z) = \frac{\gamma(2Nk, \lambda z)}{(2Nk-1)!}, \quad z > 0. \quad (7)$$

Proof. The characteristic function $\varphi_Z(w)$ of RZ in Eq. (5) is given by:

$$\begin{aligned}\varphi_Z(w) &= \mathbb{E}[e^{jwZ}] \\ &= \mathbb{E}\left[e^{jw\sum_{i=1}^{2N} X_i}\right] = (\mathbb{E}[e^{jwX_1}])^{2N} \\ &= \left(\int_0^{+\infty} e^{jwx_1} f_{X_1}(x_1) dx_1\right)^{2N} \\ &= \left(\frac{\lambda^k}{(k-1)!} \int_0^{+\infty} \underbrace{x_1^{k-1} e^{-(\lambda-jw)x_1} dx_1}_{=1}\right)^{2N}\end{aligned}\quad (8)$$

Invoking [26] (Eq. (3.381.4)) to evaluating the integral $I = \int_0^{+\infty} x_1^{k-1} e^{-(\lambda-jw)x_1} dx_1$ in Eq. (8), yields

$$\varphi_Z(w) = \left(1 - \frac{1}{\lambda} jw\right)^{-2Nk}.$$

Now, inverting Eq. (9) using the Fourier transform yields the result in Eq. (6). The CDF in (7) can be easily derived by integrating Eq. (6) over the interval $]-\infty, z]$.

Lemma 2 (Minimum of two sums of i.i.d Erlang variates). Let $X_i \sim \text{Erlang}(k, \lambda)$.

$$\begin{aligned}\text{Let } Z_1 &= \sum_{i=1}^N X_i \text{ and } Z_2 = \sum_{i=N+1}^{2N} X_i. \text{ The PDF of} \\ \text{the RV} \quad Z &= \min(Z_1, Z_2)\end{aligned}\quad (10)$$

is given by:

$$f_Z(z) = \frac{2\lambda^{Nk}}{(Nk-1)!} z^{Nk-1} e^{-\lambda z} \left(1 - \frac{\gamma(Nk, \lambda z)}{(Nk-1)!}\right), \quad z > 0. \quad (11)$$

Proof. The PDF of Z in Eq. (10) can be given by:

$$f_Z(z) = f_{Z_1}(z) (1 - F_{Z_2}(z)) + f_{Z_2}(z) (1 - F_{Z_1}(z)). \quad (12)$$

Substituting Eqs. (6)-(7) in (12) yields the result in Eq. (11).

4. P_{FA} OF THE SOCA-CFAR PROCESSOR

In this section, we derive a closed-form expression for the SOCA-CFAR processor's P_{FA} . Given the decision rule in Eq. (2) and the clutter level's estimate defined in Eq. (1), the P_{FA} can be determined as

$$\begin{aligned}P_{FA}(T) &= \mathbb{E}_Z[\Pr(X_0 > TZ \mid H_0)] \\ &= \int_0^{+\infty} \int_{TZ}^{+\infty} f_{X_0}(x) \\ &\quad | H_0) dx f_Z(z) dz\end{aligned}\quad (13)$$

Since $X_0 \sim \text{Erlang}(k, \lambda)$, Substituting its PDF $f_{X_0}(x)$ and referring to [26] (Eq. (3.381.3)), gives:

$$\frac{1}{(k-1)!} \int_0^{+\infty} \Gamma(k, \lambda Tz) f_Z(z) dz. \quad (14)$$

Now, leveraging the crucial findings presented in Section 3, we deduce, in the subsequent theorem, a closed-form expression for the P_{FA} of the SOCA-CFAR processor.

Theorem 1. The P_{FA} of the SOCA-CFAR processor under consideration is given by 15, where $(a)_n = \Gamma(a+n)/\Gamma(a)$ denotes the Pochhammer symbol, and $T_N = \frac{T}{N}$ represents the normalized scaling factor of the SOCA-CFAR processor.

$$\begin{aligned}P_{FA}(T_N) &= 2 \left(1 - \frac{\Gamma(2Nk)}{\Gamma^2(Nk) 2^{2Nk} Nk} \sum_{p=0}^{+\infty} \frac{(1)_p (Nk+k)_p}{(Nk+1)_p p! 2^p} \right. \\ &\quad - \frac{T_N^k \Gamma(k(N+1))}{\Gamma(Nk) \Gamma(k+1) (T_N+1)^{k(N+1)}} \sum_{q=0}^{+\infty} \frac{(1)_q (Nk+N)_q}{(k+1)_q q!} \left(\frac{T_N}{T_N+1}\right)^q \\ &\quad \left. + \frac{\Gamma(k(2N+1)) T_N^k}{\Gamma^2(Nk) \Gamma(k+1) Nk} \sum_{m=0}^{+\infty} \sum_{n=0}^{+\infty} \frac{(k(2N+1))_{m+n} (Nk)_m (k)_n (-1)^m (T_N)^n}{(Nk+1)_m (k+1)_n m! n!} \right)\end{aligned}\quad (15)$$

Proof. The proof is provided in Appendix A.

5. RESULTS AND DISCUSSION

This section presents numerical results related to the P_{FA} of the SOCA-CFAR and analyzes its computational properties.

5.1 Performance analysis

Figure 1 and Figure 2 show the P_{FA} performance of the SOCA-CFAR processor as a function of the normalized scaling factor T_N for different values of N . The shape parameter k is set to 1 and 5, respectively. These figures illustrate how the P_{FA} changes as the normalized scaling factor is varied, for different numbers of reference cells (N) in the CFAR processing. The choice of k implies a specific underlying statistical model for the clutter; this parameter choice affects the overall performance and could be explored further for different clutter characteristics [25-29].

The P_{FA} performance of the SOCA-CFAR processor as a function of the shape parameter k for different values of N is shown in Figures 3 and 4. In these figures, T is set to 2 and 4, respectively. These figures complement Figures 1 and 2 by examining the influence of the shape parameter, k , which directly affects the statistical model underlying the clutter. Varying k allows us to analyze the sensitivity of the SOCA-CFAR to different clutter's setups. Furthermore, by maintaining T at a constant value, we can isolate the individual effect of the shape parameter k on the P_{FA} , without interference from threshold variations.

The curves in these figures are generated using the analytical expression in Theorem 1 and show perfect agreement with the marker symbols, which are the results of Monte-Carlo simulation. This strong agreement validates both the analytical derivation and the simulation methodology, providing high confidence in the presented results.

From these figures, we can see that an increase in either the value of k or N results in a decrease in the P_{FA} . This indicates that both a less impulsive clutter (higher k) and a larger number of reference cells (N for better clutter power estimation) improve the performance of the SOCA-CFAR processor by reducing the P_{FA} . Therefore, the strategic selection of T , k and N parameters is crucial for optimizing overall system performance in practical radar applications.

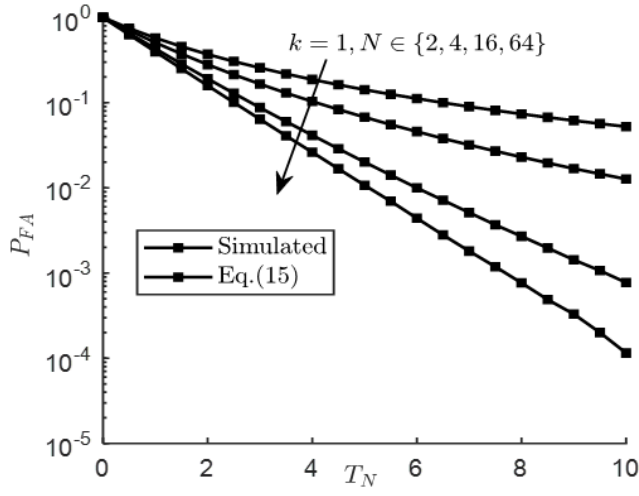


Figure 1. P_{FA} of SOCA-CFAR vs. T_N : (a) $k = 1$. The curves from top to bottom corresponds to $N=2, 4, 16$, and 64 , respectively

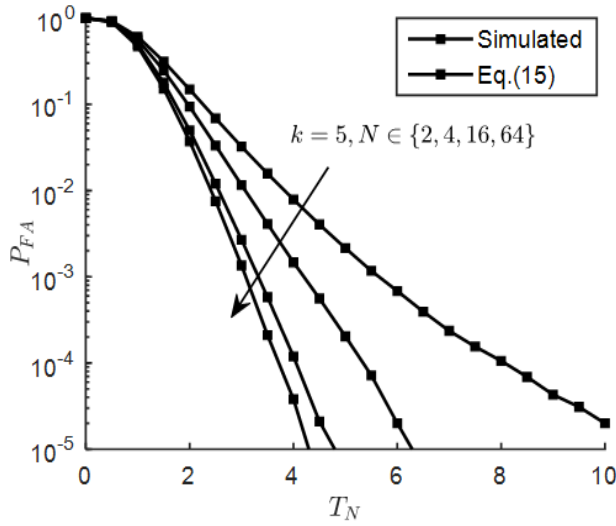


Figure 2. P_{FA} of SOCA-CFAR vs. T_N : (b) $k = 5$. The curves from top to bottom corresponds to $N = 2, 4, 16$, and 64 , respectively

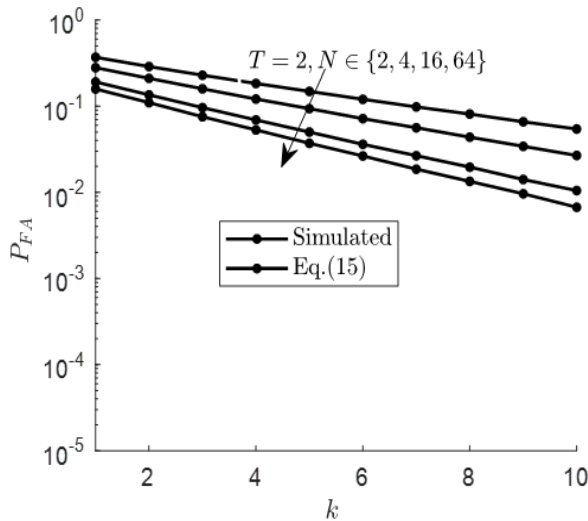


Figure 3. P_{FA} of SOCA-CFAR vs. k : (a) $T_N=2$. The curves from top to bottom corresponds to $N=2, 4, 16$, and 64 , respectively

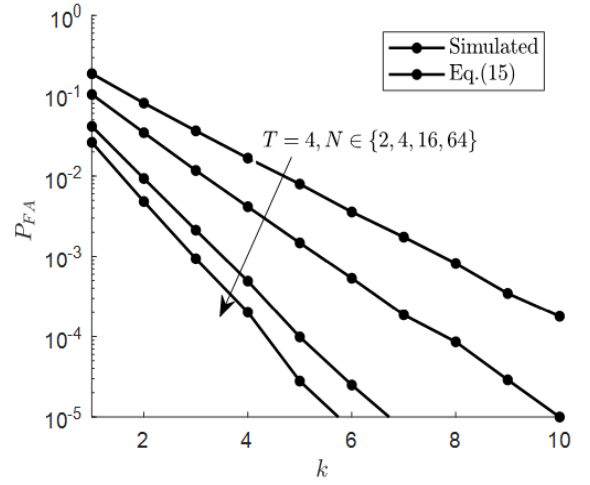


Figure 4. P_{FA} of SOCA-CFAR vs. k : (b) $T_N=4$. The curves from top to bottom corresponds to $N=2, 4, 16$, and 64 , respectively

5.2 Computational analysis

For practical implementation, the infinite series can be truncated when successive terms fall below a prescribed tolerance ϵ . Typically, 20-50 terms suffice for engineering accuracy ($\epsilon = 10^{-6}$).

Remark: The expression reduces to known results for special cases:

- $N = 1, k = 1$: Classical CA-CFAR with $P_{FA} = (1 + T_1)^{-1}$ -Large N limit: Approaches Gaussian approximation.

Proposition 1 (Convergence Properties) *All infinite series in Theorem 1 converge absolutely for $T_N > 0, N \geq 1$, and $k > 0$.*

Proof. The convergence follows from:

1. For the series in p : $\left| \frac{(1)p^{(Nk+k)p}}{(Nk+1)p!2^p} \right| \sim \mathcal{O}(p^{-1})$ as $p \rightarrow \infty$.
2. For the series in q : geometric convergence with ratio $|T_N/(T_N + 1)| < 1$.
3. For the double series: dominated convergence via $\sum_{m,n} |a_{m,n}| \leq \sum_{m,n} \frac{C^{m+n}}{m!n!} < \infty$ for some constant C .

6. CONCLUSION

In this letter, we have assessed the performance of the SO-CFAR processor in the context of a clutter environment characterized by an Erlang distribution. To do so, we have derived the necessary statistics for the clutter's mean level in a form of the sum and the minimum sum of independent and identically distributed (i.i.d) Erlang random variates' PDFs. Based on that we have then derived a closed-form expression for the SO-CFAR processor's P_{FA} . Furthermore, aside from its ease of evaluation, this closed-form expression can also be instrumental in facilitating a realistic design and analysis of the SO-CFAR processor. Additionally, an examination of various parameters and their influence on the performance of the processor has been conducted. The numerical findings indicate that an augmentation in either the clutter's shape parameter λ , or the size of the reference window N , results in an enhancement of the processor's performance. Future work

should investigate SO-CFAR performance in heterogeneous environments (clutter edges, multiple targets), conduct comparative studies with other CFAR variants, and validate results using real radar data.

ACKNOWLEDGEMENTS

This research was supported by the Researchers Supporting Project (PNURSP2025R120) at Princess Nourah bint Abdulrahman University, Riyadh, Saudi Arabia.

REFERENCES

- [1] Gandhi, P.P., Kassam, S.A. (2002). Analysis of CFAR processors in nonhomogeneous background. *IEEE Transactions on Aerospace and Electronic Systems*, 24(4): 427-445. <http://dx.doi.org/10.1109/7.7185>
- [2] Dai, Z., Wang, P., Wei, H., Xu, Y. (2019). Adaptive detection with constant false alarm ratio in a non-Gaussian noise background. *IEEE Communications Letters*, 23(8): 1369-1372. <http://dx.doi.org/10.1109/LCOMM.2019.2918816>
- [3] Wang, H., Hu, T., Li, T., Wu, D., Xu, Z., Xu, X., Tian, Z. (2023). Intelligent interference waveform design for radar detection based on the cross-correlation value function. *IEEE Transactions on Aerospace and Electronic Systems*, 60(2): 2061-2070. <http://dx.doi.org/10.1109/TAES.2023.3347679>
- [4] Zhou, J., Xie, J. (2023). Performance analysis of linearly combined order statistics CFAR processors in heterogeneous background. *IEEE Transactions on Aerospace and Electronic Systems*, 60(2): 2428-2437. <https://doi.org/10.1109/TAES.2023.3339405>
- [5] Chen, Z., Chen, A., Liu, W., Ma, X. (2023). CFAR detection in nonhomogeneous Weibull sea clutter for skywave OTHR. *IEEE Geoscience and Remote Sensing Letters*, 20: 1-5. <http://dx.doi.org/10.1109/LGRS.2023.3313179>
- [6] Mboungam, A.H.M., Zhi, Y., Monguen, C.K.F. (2024). Clutter map constant false alarm rate mixed with the Gabor transform for target detection via Monte Carlo simulation. *Applied Sciences*, 14(7): 2967. <https://doi.org/10.3390/app14072967>
- [7] Gandhi, P.P., Kassam, S.A. (1994). Optimality of the cell averaging CFAR detector. *IEEE Transactions on Information Theory*, 40(4): 1226-1228. <https://doi.org/10.1109/18.335950>
- [8] Yan, B., Roberts, I.P. (2025). Advancements in millimeter-wave radar technologies for automotive systems: A signal processing perspective. *Electronics*, 14(7): 1436. <https://doi.org/10.3390/electronics14071436>
- [9] Hansen, V.G., Sawyers, J.H. (1980). Detectability loss due to "greatest of" selection in a cell-averaging CFAR. *IEEE Transactions on Aerospace and Electronic Systems*, 1(1): 115-118. <https://doi.org/10.1109/TAES.1980.308885>
- [10] Trunk, G.V. (1978). Range resolution of targets using automatic detectors. *IEEE Transactions on Aerospace and Electronic Systems*, 15(5): 750-755. <https://doi.org/10.1109/TAES.1978.308625>
- [11] Alvarado, M.C.L., García, F.D.A., Jiménez, L.P.J., Fraidenraich, G., Iano, Y. (2022). Performance evaluation of SOCA-CFAR detectors in Weibull-distributed clutter environments. *IEEE Geoscience and Remote Sensing Letters*, 19: 1-5. <https://doi.org/10.1109/LGRS.2022.3152936>
- [12] Kerbaa, T.H., Mezache, A., Oudira, H. (2022). Improved decentralized SO-CFAR and GO-CFAR detectors via moth flame algorithm. In *2022 International Conference of Advanced Technology in Electronic and Electrical Engineering (ICATEEE)*, M'sila, Algeria, pp. 1-5. <https://doi.org/10.1109/ICATEEE57445.2022.10093725>
- [13] Jiménez, L.P.J., García, F.D.A., Alvarado, M.C.L., Fraidenraich, G., De Lima, E.R. (2022). A general CA-CFAR performance analysis for weibull-distributed clutter environments. *IEEE Geoscience and Remote Sensing Letters*, 19: 1-5. <https://doi.org/10.1109/LGRS.2022.3187554>
- [14] Rohling, H. (2007). Radar CFAR thresholding in clutter and multiple target situations. *IEEE Transactions on Aerospace and Electronic Systems*, 43(4): 608-621. <https://doi.org/10.1109/TAES.1983.309350>
- [15] Zhu, J.C., Huang, X.H., Liu, J.Y., Deng, Z.M. (2024). Robust CFAR detector based on CLEAN for sidelobe suppression. *IEEE Sensors Journal*, 24(8): 12345-12356. <https://doi.org/10.1109/JSEN.2024.3382137>
- [16] Guida, M., Longo, M., Lops, M. (1993). Biparametric CFAR procedures for lognormal clutter. *IEEE Transactions on Aerospace and Electronic Systems*, 29(3): 798-809. <https://doi.org/10.1109/7.220931>
- [17] Rifkin, R. (2002). Analysis of CFAR performance in Weibull clutter. *IEEE Transactions on Aerospace and Electronic Systems*, 38(2): 315-329. <https://doi.org/10.1109/7.722257>
- [18] Watts, S. (1996). Cell-averaging CFAR gain in spatially correlated K-distributed clutter. *IEEE Proceedings-Radar, Sonar and Navigation*, 143(5): 321-327. <https://doi.org/10.1049/ip-rsn:19960745>
- [19] Tsakalides, P., Trinic, F., Nikias, C.L. (2000). Performance assessment of CFAR processors in Pearson-distributed clutter. *IEEE Transactions on Aerospace and Electronic Systems*, 36(4): 1377-1386. <http://dx.doi.org/10.1109/7.892685>
- [20] Weinberg, G.V. (2013). Constant false alarm rate detectors for Pareto clutter models. *IET Radar, Sonar & Navigation*, 7(2): 153-163. <https://doi.org/10.1049/iet-rsn.2011.0374>
- [21] Aalo, V.A., Peppas, K.P., Efthymoglou, G. (2015). Performance of CA-CFAR detectors in nonhomogeneous positive alpha-stable clutter. *IEEE Transactions on Aerospace and Electronic Systems*, 51(3): 2027-2038. <https://doi.org/10.1109/TAES.2015.140043>
- [22] García, F.D.A., Rodriguez, A.C.F., Fraidenraich, G., Santos Filho, J.C.S. (2018). CA-CFAR detection performance in homogeneous Weibull clutter. *IEEE Geoscience and Remote Sensing Letters*, 16(6): 887-891. <https://doi.org/10.1109/LGRS.2018.2885451>
- [23] Zhou, W., Xie, J., Li, G., Du, Y. (2017). Robust CFAR detector with weighted amplitude iteration in nonhomogeneous sea clutter. *IEEE Transactions on Aerospace and Electronic Systems*, 53(3): 1520-1535. <https://doi.org/10.1109/TAES.2017.2671798>
- [24] Zhou, W., Xie, J., Zhang, B., Li, G. (2018). Maximum likelihood detector in gamma-distributed sea clutter.

IEEE Geoscience and Remote Sensing Letters, 15(11): 1705-1709.

<https://doi.org/10.1109/LGRS.2018.2859785>

- [25] Sahed, M., Kenane, E., Khalfa, A., Djahli, F. (2022). Exact closed-form P fa expressions for CA-and GO-CFAR detectors in Gamma-distributed radar clutter. IEEE Transactions on Aerospace and Electronic Systems, 59(4): 4674-4679. <https://doi.org/10.1109/TAES.2022.3232101>
- [26] Gradshteyn, I.S., Ryzhik, I.M. (2014). Table of integrals, series, and products. Academic Press. <http://dx.doi.org/10.1119/1.15756>
- [27] Abramowitz, M., Stegun, I.A. (1948). Handbook of mathematical functions with formulas, graphs, and mathematical tables. US Government Printing Office, Vol. 55. <http://doi.org/10.1119/1.15378>
- [28] Olver, F.W.J., Lozier, D.W., Boisvert, R.F., Clark, C.W. (2010). NIST Handbook of Mathematical Functions. Cambridge University Press. <https://dl.acm.org/doi/10.5555/1830479>
- [29] Conte, E., De Maio, A., Galdi, C. (2004). Statistical analysis of real clutter at different range resolutions. IEEE Transactions on Aerospace and Electronic Systems, 40(3): 903-918. <https://doi.org/10.1109/TAES.2004.1337463>

NOMENCLATURE

$(a)_s$	Pochhammer's symbol [27](Eq. (5.2.4))
$f_X(x)$	Probability Density Function (PDF)
$F_X(x)$	Cumulative Distribution Function (CDF)
$E[X]$	Expectation of the random variable X
$\Gamma(\cdot)$	Gamma function [26], Eq. (8.310.1)
$\Gamma(\cdot, \cdot)$	Upper incomplete Gamma function [26], Eq. (8.350.2)
$\gamma(\cdot, \cdot)$	Lower incomplete Gamma function [26], Eq. (8.350.1)

APPENDIX A

Proof of the theorem1

Step I: Integral Decomposition

According lemma 2, the PDF $f_Z(z)$ in the case of SOCA-CFAR is given by Eq. (11). Now, Substituting Eq. (11) into Eq. (14) with $T = T_N N$ yields:

$$P_{FA}(T_N) = I_1 - I_2 \quad (A.1)$$

where,

$$I_1 = \frac{2\lambda^{Nk}}{(k-1)!(Nk-1)!} \int_0^\infty \Gamma(k, \lambda T_N N z) z^{Nk-1} e^{-\lambda z} dz \quad (A.2)$$

$$I_2 = \frac{2\lambda^{Nk}}{(k-1)![(Nk-1)!]^2} \int_0^\infty \Gamma(k, \lambda T_N N z) z^{Nk-1} e^{-\lambda z} \gamma(Nk, \lambda z) dz \quad (A.3)$$

Step II: Evaluation of I_1

For integer k , the upper incomplete gamma function admits the series representation [27] (Eq. (8.352)):

$$\Gamma(k, x) = (k-1)! e^{-x} \sum_{j=0}^{k-1} \frac{x^j}{j!} \quad (A.4)$$

Substituting Eq. (A.5) into (A.3):

$$I_1 = \frac{2\lambda^{Nk}}{(Nk-1)!} \sum_{j=0}^{k-1} \frac{(\lambda T_N N)^j}{j!} \int_0^\infty z^{Nk+j-1} e^{-\lambda(1+T_N N)z} dz \quad (A.5)$$

Applying the standard gamma integral [26] (Eq. 3.381.4):

$$\int_0^\infty t^{n-1} e^{-at} dt = \frac{\Gamma(n)}{a^n}, \quad \text{Re}(a) > 0, \text{Re}(n) > 0 \quad (A.6)$$

yields:

$$I_1 = \frac{2\Gamma(k)\Gamma(Nk)}{\lambda^{Nk}(1+T_N N)^{Nk}} \sum_{j=0}^{k-1} \frac{(Nk)_j}{j!} \left(\frac{T_N N}{1+T_N N} \right)^j \quad (A.7)$$

The series in Eq. (A.8) can be expressed using the confluent hypergeometric function:

$$\sum_{j=0}^\infty \frac{(a)_j}{j!} z^j = {}_1F_1(a; 1; z) \quad (A.8)$$

Applying Kummer's transformation [28] (Eq. (1.5.3)):

$${}_1F_1(a; b; z) = e^z {}_1F_1(b-a; b; -z) \quad (A.9)$$

and utilizing connection formulas for hypergeometric functions [28], Eq. (1.5.7), we obtain:

$$I_1 = 2 \left(1 - \frac{\Gamma(2Nk)}{\Gamma^2(Nk)2^{2Nk}Nk} \sum_{p=0}^\infty \frac{(1)_p(Nk+k)_p}{(Nk+1)_p p! 2^p} \right) \quad (A.10)$$

Step III: Evaluation of I_2

Using the series representation of the lower incomplete gamma function [27] (Eq. (6.5.29)):

$$\gamma(Nk, x) = x^{Nk} e^{-x} \sum_{m=0}^\infty \frac{x^m}{\Gamma(Nk+m+1)} \quad (A.11)$$

Substituting Eq. (A.11) into Eq. (A.3):

$$I_2 = \frac{\lambda^{Nk}}{(Nk-1)!} \sum_{m=0}^\infty \frac{\lambda^m}{\Gamma(Nk+m+1)} \int_0^\infty \Gamma(k, \lambda T_N N z) z^{2Nk+m-1} e^{-2\lambda z} dz \quad (A.12)$$

Expanding $\Gamma(k, \lambda T_N N z)$ using Eq. (A.4) and integrating term-by-term:

$$I_2 = \frac{\Gamma(k)}{2^{2Nk}(Nk-1)!} \sum_{m=0}^{\infty} \sum_{n=0}^{\infty} \frac{T_N^n \Gamma(2Nk+m+n)}{n! \Gamma(Nk+m+1) 2^{m+n}} \quad (\text{A.13})$$

The double series in Eq. (A.13) can be decomposed using gamma function identities [27] (Eq. 6.1.15) and Pochhammer symbol properties [27] (Eq. 6.1.22):

$$I_2 = I_{2a} - I_{2b} \quad (\text{A.14})$$

where,

$$I_{2a} = \frac{T_N^k \Gamma(k(N+1))}{\Gamma(Nk) \Gamma(k+1) (T_N+1)^{k(N+1)}} \quad (\text{A.15})$$

$$\sum_{q=0}^{\infty} \frac{(1)_q (Nk+N)_q}{(k+1)_q q!} \left(\frac{T_N}{T_N+1} \right)^q$$

$$I_{2b} = \frac{\Gamma(k(2N+1)) T_N^k}{\Gamma^2(Nk) \Gamma(k+1) Nk} \sum_{m,n=0}^{\infty} \frac{(k(2N+1))_{m+n} (Nk)_m (k)_n (-1)^m T_N^n}{(Nk+1)_m (k+1)_n m! n!} \quad (\text{A.16})$$

Step IV: Final Assembly

Combining results from Steps II and III using Eq. (A.1):

$$P_{\text{FA}}(T_N) = I_1 - I_{2a} + I_{2b} \quad (\text{A.17})$$

Substituting Eq. (A.10), Eq. (A.15), and Eq. (A.16) yields the theorem statement.